THE GLOBAL FLOW OF THE MANEV PROBLEM

J. Delgado, F.N. Diacu, E.A. Lacomba,
A. Mingarelli, V. Mioc, E. Perez
and
C. Stoica

DMS-716-IR **September 1995**

THE GLOBAL FLOW OF THE MANEV PROBLEM

Joaquín DELGADO[1], Florin N. DIACU[2], Ernesto A. LACOMBA[1]
Angelo MINGARELLI[3], Vasile MIOC[4], Ernesto PEREZ[1], Cristina STOICA[5]

[1] *Departamento de Matemáticas*
Universidad Autónoma Metropolitana-Iztapalapa
Apdo. 55534, México, D.F., México

[2] *Department of Mathematics and Statistics*
University of Victoria
Victoria, British Columbia, V8W 3P4, Canada

[3] *Department of Mathematics and Statistics*
Carleton University
Ottawa, Ontario, K1S 5B6, Canada

[4] *Institutul Astronomic al Academiei Române*
Observatorul Astronomic
Str. Cireşilor 19; 3400 Cluj-Napoca, România

[5] *Institutul de Gravitaţie şi Ştiinţe Spaţiale*
Laboratorul de Gravitaţie
Bd. Ana Ipătescu 21; 71111 Bucureşti, România

Abstract

The Manev problem (a two-body problem given by a potential of the form $A/r + B/r^2$, where r is the distance between particles and A, B are positive constants) comprises several important physical models, having its roots in research done by Isaac Newton. We provide its analytic solution, then completely describe its global flow using McGehee coordinates and topological methods, and offer the physical interpretation of all solutions. We prove that if the energy constant is negative, the orbits are, generically, precessional ellipses, except for a zero-measure set of initial data, for which they are ellipses. For zero energy, the orbits are precessional parabolas, and for positive energy they are precessional hyperbolas. In all these cases, the set of initial data leading to collisions has positive measure. Using KAM theory, we show that Manev's model is a natural framework for the solar system.

I. INTRODUCTION

The question we fully answer in this paper has a long history. We deal with a two-body problem given by a potential of the form $A/r+B/r^2$, where r is the distance between particles and A, B are positive constants. Newton was the first to consider it in his *Principia*. In Book I, Article IX, Theorem IV, Corollary 2, he claimed that such a force leads to a *precessionally elliptic* relative orbit; this means that, with respect to a fixed frame having one particle at the origin, the other particle moves on an ellipse that rotates in its plane of motion. This was the only result Newton published in connection with this gravitational model, but he tackled it for many years to follow his first edition of *Principia*. The 1888-catalogue of the Portsmouth Collection of unpublished manuscripts that are stored today in the library of Cambridge University, shows Newton's interest in this model; it was aroused by the difficulties he encountered in trying to explain the apsidal motion of the moon within the framework of the inverse-square-force model. After Newton, the $A/r + B/r^2$-potential was tackled by Clairaut, who finally abandoned it in favor of the classical one.

Using physical principles, the Bulgarian physicist Manev[1] (or Maneff—in French and German spelling) obtained a similar potential during the third decade of our century. Assigning the mass M to the particle at the origin, the unit mass to the rotating particle and denoting $\mu = GM, \beta = A/\mu - 1, \gamma = 2B/\mu$, where G is the constant of gravitation, Manev's potential corresponds to the values $\beta = 0, \gamma = 3\mu/c^2$ of the constants, where c is the speed of light. This model allowed a good theoretical justification of the perihelion advance of Mercury and of the other inner planets as well as an accurate description of the moon's motion.

The main goal of this paper is to emphasize a new point of view concerning the qualitative behavior of orbits in the solar system modeled by a Manev-type law of motion. The classical point of view is that the orbit of celestial objects around the sun must be an ellipse, a parabola, or a hyperbola (depending on the initial data). But because of the perturbation of the other objects in the system, the orbit is in fact a precessional ellipse, parabola, or hyperbola. Unfortunately, this classical point of view encounters difficulties: the theoretical calculations do not fit the observations, and this happens especially for celestial objects coming close to the sun. The perihelion advance of Mercury and of the other inner planets cannot be explained within the the framework of the Newtonian theory.

The new point of view is that we can maintain the study of the solar system within the framework of classical mechanics by substituting Newton's model with the one of Manev. Of help in this sense are the results of the KAM theory. As it has been shown in a paper by Lacomba, Llibre and Nunes[2], if the equations of motion describing Manev's problem are slightly perturbed by some external force, which *does not have to be* Hamiltonian, "most" invariant cylinders and tori are (topologically) preserved under this perturbation. From the physical point of view this means that the natural (unperturbed) orbit of a celestial object around the sun is not an ellipse, parabola, or hyperbola, but a precessional

ellipse, precessional parabola, or precessional hyperbola, the precessional effect becoming more evident the closer the orbit is to the sun. Under the perturbation of the other celestial objects, the orbit continues to remain, in general, a precessional ellipse, precessional parabola, or precessional hyperbola.

Several other Manev-type models have recently been the subject of research. Mioc[3] has considered Fock's relativistic field, truncating the negligible terms and obtaining the values $\beta = 2(E^2-1), \gamma = 6\mu E^2/c^2$ of the parameters, where $E = 1+h/c^2$ and h is the total energy per unit mass of the rotating particle. Saslaw[4], and later Mioc and Radu[5], have considered the motion in the photogravitational field generated by a source of radiation, taking the values $\beta = -\sigma L/(4\pi\mu mc), \gamma = 0$ of the parameters, where σ and m are the cross-sectional area and the mass of the rotating body and L is the luminosity of the central body. The two-body problem with equivalent gravitational parameter ($\beta \neq 0, \gamma = 0$) has been considered by Şelaru, Cucu-Dumitrescu and Mioc[6].

There are other directions of research where this potential occurs: the oblate planet problem for example is approximated by the same potential[7]; Ureche[8] analysed the astrophysical problem of the free-fall collapse of a homogeneous sphere; Diacu[9] considered generalizations to the three-body problem in the more general mathematical context of *quasihomogeneous potentials*, showing that Manev's case represents the only bifurcation of the flow in the quasihomogeneous case. Diacu[10] also studied the gravitational isosceles three-body case, pointing out possible applications in atomic physics.

The general case of the Manev potential for any positive values of the constants A and B has been considered, in Hamiltonian formulation, for negative total energy, by Lacomba, Llibre and Nunes (see ref. 2), who have also applied KAM (Kolmogorov-Arnold-Moser) theory to a perturbed Manev-potential, to prove the invariance of nonresonant cylinders and tori. They also computed the Melnikov integral associated with the nonhyperbolic equilibria. The analytic solution and the local flow of the Manev model near collision has been obtained by Diacu, Mingarelli, Mioc and Stoica[11]. The more complicated anisotropic Manev problem (important for understanding the connections between classical and quantum mechanics) has been recently investigated by Craig, Diacu, Lacomba and Perez[12], who have fully understood the flow near collision and have described some elements of the global flow, obtaining in particular the complete picture of the zero energy case.

The goal of this paper is to provide the complete analytic, geometric, and physical description of the Manev problem. In Sections II, III, and IV, we compute the analytic solution, which, from the practical point of view, can be used in numerical endeavors. Unfortunately, the complicated closed form of the solution hides the nice properties of the model. Therefore we continue with a qualitative analysis, which reveals the geometrical nature of the orbits. In Section V we use the McGehee technique[13] to blow up the collision singularity and offer new, regularized, equations of motion. The main idea of this method is to paste, instead of the collision singularity, a manifold to the phase space. This manifold, though now part of the phase space, has nothing to do with the real physical orbits. Its advantage, however, is that, due to the continuity of solutions with respect to the initial

data, it provides information about orbits passing close to collision. The study of the (fictitious) flow on the collision manifold is therefore important for the understanding of the local flow near collision. In this case, however, the regularized equations of motion allow us to provide a full description of the global flow. The flow on the torus is formed by periodic orbits, except the upper and lower circle, which are formed by degenerate equilibria. We observe that the global flow has a rotational symmetry, which we use to reduce the dimension of the phase space. In this reduced phase space, the collision manifold is a circle of equilibria: two of these equilibria correspond tho the circles of equilibria on the torus, while all the others correspond to the periodic orbits on the torus (see Figure 2).

In Section VI we treat the negative-energy case. Every energy level is a spherical cap (which is obviously topologically equivalent with a disk—see Figure 3). There are infinitely many heteroclinic orbits connecting the equilibria of the collision circle, two homoclinic orbits, and infinitely many periodic orbits. The heteroclinic and homoclinic solutions physically correspond to orbits ejecting from a collision and also ending in a collision. The periodic orbits correspond to tori of solutions in phase space. In Section VII we prove that most of the tori of solutions correspond to quasiperiodic orbits (precessional ellipses), while a set of measure zero of initial data leads to elliptic orbits. In Section VIII we study the zero-energy and positive-energy cases. Each energy level is topologically equivalent with an annulus: in the zero-energy case it is a paraboloid with the cap removed (see Figure 4), while in the positive-energy case, depending on the initial data, it is part of a hyperboloid of one sheet (see Figure 5a), one sheet of a cone of two sheets with the cap removed (see Figure 5b), or one sheet of a hyperboloid of two sheets with the cap removed (see Figure 5c). All these surfaces are bordered by the collision circle. From the physical point of view, the zero-energy case solutions correspond to precessional parabolas, whereas the positive-energy ones correspond to precessional branches of hyperbolas. In all cases, and in general, the set of initial data leading to collisions has positive measure. Also, as we have proved in ref. 11, the collision is not regularizable, in the sense that continuity with respect to the initial data gets lost after collision.

The main conclusion to be drawn in this paper, from the point of view of applications, is that the natural, unperturbed motion in the solar system is precessional, as relativity has already shown. But as we can see, to prove this we do not need the powerful tool of relativity. To fully understand (both quantitatively and qualitatively) the motion of the solar system, we can remain in the framework of classical mechanics by using Manev's model.

II. THE RADIUS VECTOR—DIRECT APPROACH

The Manev problem is described by a Hamiltonian system, i.e. a system of the type:

$$\dot{\mathbf{q}} = \partial H(\mathbf{p}, \mathbf{q})/\partial \mathbf{p}, \quad \dot{\mathbf{p}} = -\partial H(\mathbf{p}, \mathbf{q})/\partial \mathbf{q},$$

where the Hamiltonian function H has the property $H(\mathbf{p}, \mathbf{q}) = h$ (constant), i.e. it is a

first integral (called the integral of energy) of the system.

In our case, the Hamiltonian H is given by

$$H(\mathbf{p},\mathbf{q}) = (1/2)\left(|\mathbf{p_1}|^2 + |\mathbf{p_2}|^2\right) - A/|\mathbf{q}_1 - \mathbf{q}_2| - B/|\mathbf{q}_1 - \mathbf{q}_2|^2,$$

where we have denoted by $\mathbf{q} = (\mathbf{q_1}, \mathbf{q_2})$ the *configuration* of the system of two particles and by $\mathbf{p} = (\mathbf{p_1}, \mathbf{p_2})$ the *momentum*, A, B being positive constants.

Since H depends only on the relative positions $\mathbf{q}_1 - \mathbf{q}_2$ and not on the position vectors $\mathbf{q}_1$ and $\mathbf{q}_2$, we can reduce the Manev problem to a central force problem by introducing the relative coordinates $\mathbf{r} = \mathbf{q}_1 - \mathbf{q}_2$, which transform the Hamiltonian into:

$$H(\mathbf{p},\mathbf{r}) = (1/2)|\mathbf{p}|^2 - A/|\mathbf{r}| - B/|\mathbf{r}|^2.$$

We will use this formulation of the problem in our qualitative endeavors (Sections V-VIII). To obtain the analytic expression of the solution (Sections II-IV), we eliminate the momentum from the above equations and express them as a second order system of the form

$$\ddot{\mathbf{r}} = -(1+\beta)\mu\mathbf{r}/r^3 - \gamma\mu\mathbf{r}/r^4, \tag{2.1}$$

where $\beta = A/\mu - 1, \gamma = 2B/\mu, \mu = GM$, G is the gravitational constant, $\beta = A/\mu - 1$, $\gamma = 2B/\mu$, $\mu = GM$, G is the gravitational constant, M is the mass of one particle, the other having mass 1, and $r = |\mathbf{r}|$.

Using polar coordinates (r, u), the equations (2.1) become

$$\begin{cases} \ddot{r} - r\dot{u}^2 = -(\mu/r^2)(1+\beta+\gamma/r) \\ r\ddot{u} + 2\dot{r}\dot{u} = 0. \end{cases} \tag{2.2}$$

Let us attach to the equations (2.2) the initial conditions

$$(r, u, \dot{r}, \dot{u})(t_0) = (r_0, u_0, V_0\cos\psi, V_0\sin\psi/r_0),$$

where $V_0 = V(t_0), V = |\dot{\mathbf{r}}|$, and ψ is the angle between the initial radius vector and the initial velocity. Since the force-field is central, the angular momentum is conserved, so the second equation in (2.2) yields the integral

$$r^2\dot{u} = C, \tag{2.3}$$

where $C = r_0V_0\sin\psi$ is the constant of the angular momentum. The integral of energy is

$$V^2 = \dot{r}^2 + r^2\dot{u}^2 = (\mu/r)[2(1+\beta) + \gamma/r] + h, \tag{2.4}$$

where h is the energy constant.

The rectilinear case (which corresponds to the zero angular momentum, $C = 0$) is easy to solve. The phase-space picture is given in Figure 1. (In fact, we will recover these orbits

in the qualitative analysis performed in Sections V-VIII.) Throughout Sections II-IV, we will assume $C \neq 0$.

Figure 1.
(a) The case $h < 0$, where $r_0 = (-A - \sqrt{A^2 - 2Bh})/h$;
(b) The case $h = 0$; (c) The case $h > 0$.

Using the relation $dt = (r^2/C)du$ obtained from (2.3), the first equation in (2.1) takes the Binet-type form

$$\frac{d^2(1/r)}{du^2} + (1 - \gamma\mu/C^2)(1/r) = (1+\beta)\mu/C^2, \tag{2.5}$$

with the initial conditions

$$(r, \frac{d(1/r)}{du})(u_0) = (r_0, -\frac{1}{r_0 \tan\psi}).$$

The solution of the initial value problem attached to the equations (2.5) depends on the value of the constant $\alpha = \gamma\mu/C^2$. We distinguish 3 cases: (a) $\alpha < 1$, (b) $\alpha = 1$, and (c) $\alpha > 1$:

$$r = \Big[\Big(\frac{1}{r_0} - \frac{(1+\beta)\mu}{(1-\alpha)C^2}\Big)C_\alpha(u) - \frac{S_\alpha(u)}{r_0\tan\psi} + \frac{(1+\beta)\mu}{(1-\alpha)C^2}\Big]^{-1}, \tag{2.6a}$$

$$r = \Big[\frac{(1+\beta)\mu(u-u_0)^2}{2C^2} - \frac{u-u_0}{r_0\tan\psi} + \frac{1}{r_0}\Big]^{-1}, \tag{2.6b}$$

$$r = \Big[\Big(\frac{1}{r_0} + \frac{(1+\beta)\mu}{(\alpha-1)C^2}\Big)\tilde{C}_\alpha(u) - \frac{\tilde{S}_\alpha(u)}{r_0\tan\psi} - \frac{(1+\beta)\mu}{(\alpha-1)C^2}\Big]^{-1}, \tag{2.6c}$$

where

$$S_\alpha(u) = (1-\alpha)^{-\frac{1}{2}}\sin(\sqrt{1-\alpha}(u-u_0)),$$
$$C_\alpha(u) = \cos(\sqrt{1-\alpha}(u-u_0)),$$
$$\tilde{S}_\alpha(u) = (1-\alpha)^{-\frac{1}{2}}\sinh(\sqrt{\alpha-1}(u-u_0)),$$
$$\tilde{C}_\alpha(u) = \cosh(\sqrt{\alpha-1}(u-u_0)).$$

III. THE ORBITAL ELEMENTS—PERTURBATIVE APPROACH

Let us now isolate the Newtonian attraction term per unit mass, $-\mu\mathbf{r}/r^3$, in the right hand side of the equations (2.1), and treat the remaining term $-\beta\mu\mathbf{r}/r^3 - \gamma\mu\mathbf{r}/r^4$ as a perturbing acceleration. In this way we can tackle the problem in the frame of the classical perturbation theory.

According to this theory, developed primarily by Lagrange and based on the variation of parameters[14], the real (perturbed) trajectory can be regarded as the envelope of a family

of osculating Keplerian orbits (conic sections) whose initial conditions change continuously. The motion will then be described by a set of relations between the Keplerian orbital elements, their time-derivatives, and time; these form the so-called Newton-Euler or Gauss equations[15]. If the components of the perturbing accelerations (which appear in these equations) do not contain the time explicitly, one can choose another independent variable: one of the anomalies (as in ref. 15, p. 157) or the argument of latitude.

We will further express the trajectory of the particle with respect to the time dependent osculating Keplerian orbital elements: a = *the semimajor axis*, Ω = *the longitude of the ascending node*, i = *the inclination*, e = *the eccentricity*, ω = *the argument of the pericentre*, and u = *the argument of the latitude*. We will also use $p = a(1-e^2)$ = *the semilatus rectum*, $v = u - \omega$ = *the true anomaly*, and the parameters $q = e\cos\omega$, $k = e\sin\omega$, which are suitable for the study of small-eccentricity orbits (those close to circles), for which the pericentre is unwell—or not at all—defined[16].

Let S, T, W denote the radial, transverse, and binormal components of the perturbing acceleration, respectively. Since they do not depend explicitly on the time t, we can describe the perturbed motion by means of the Newton-Euler equations written with respect to u in the form (see e.g. ref. 5):

$$\begin{cases} p' &= 2(Z/\mu)r^3T \\ \Omega' &= (Z/\mu)r^3W\frac{\sin u}{p\sin i} \\ i' &= (Z/\mu)r^3W\frac{\cos u}{p} \\ q' &= (Z/\mu)\{r^3kW\sin u\frac{\cot i}{p} + r^2T[r\frac{q+\cos u}{p} + \cos u] + r^2S\sin u\} \\ k' &= (Z/\mu)\{-r^3qW\sin u\frac{\cot i}{p} + r^2T[r\frac{k+\sin u}{p} + \sin u] - r^2S\cos u\} \\ t' &= Zr^2/\sqrt{\mu p}, \end{cases} \tag{3.1}$$

where $(' = \frac{d}{du}$ and $Z = (1 - r^2\dot{\Omega}\frac{\cos i}{\sqrt{\mu p}})^{-1})$, with the initial conditions

$$(p, \Omega, i, q, k, t)(u_0) = (p_0, \Omega_0, i_0, q_0, k_0, t_0).$$

Since the perturbing force in the equations (2.1) is radial, the components of the perturbing acceleration are $S = -(\mu/r^2)(\beta + \gamma/r)$, $T = W = 0$. Also notice that $Z = 1$. Replacing these values into the equations (3.1), we obtain

$$\begin{cases} p' = \Omega' = i' = 0, \\ q' = -(\beta + \gamma/r)\sin u \\ k' = (\beta + \gamma/r)\cos u \\ t' = r^2/\sqrt{\mu p}. \end{cases} \tag{3.2}$$

Integrating the first three equations and using the initial data, we obtain that all along the motion $p = p_0$, $\Omega = \Omega_0$, and $i = i_0$, which means that the *semilatus rectum* is constant and the motion is planar.

According to the perturbation theory we use, we may describe the real trajectory by the equation of a conic section $r = p/(1 + e\cos v)$, whose parameters are functions of u.

From the definition of q and k, the relation $v = u - \omega$, and the constancy of p, this equation becomes

$$r(u) = \frac{p_0}{(1 + q\cos u + k\sin u)}. \tag{3.3}$$

On the other hand, since for osculating conic sections $p = p_0 =$ constant (the same constant as in the Kepler problem) and C has the same value as in the Kepler problem[17] (given by $C^2/\mu = p$), we put $C^2 = \mu p_0$, which—according to the previous section—leads to $\alpha = \gamma/p_0$. With this expression for α, and with (3.3), the coupled equations for q and k in (3.1) have the exact solution, for (a) $\alpha < 1$, (b) $\alpha = 1$, (c) $\alpha > 1$, respectively:

$$\begin{cases} q(u) = \{S_\alpha(u)[\sin(u-u_0) - \alpha\cos u_0 \sin u] + C_\alpha(u)\cos(u-u_0)\}q_0 + \\ \qquad \{S_\alpha(u)[\cos(u-u_0) - \alpha\sin u_0 \sin u] - C_\alpha(u)\sin(u-u_0)\}k_0 - \\ \qquad (\alpha+\beta)S_\alpha(u)\sin u + [(\alpha+\beta)/(1-\alpha)][1 - C_\alpha(u)]\cos u, \\ k(u) = \{-S_\alpha(u)[\cos(u-u_0) - \alpha\cos u_0 \cos u] + C_\alpha(u)\sin(u-u_0)\}q_0 + \\ \qquad \{S_\alpha(u)[\sin(u-u_0) + \alpha\sin u_0 \cos u] + C_\alpha(u)\cos(u-u_0)\}k_0 + \\ \qquad (\alpha+\beta)S_\alpha(u)\cos u + [(\alpha+\beta)/(1-\alpha)][1 - C_\alpha(u)]\sin u, \end{cases} \tag{3.4a}$$

$$\begin{cases} q(u) = [\cos(u-u_0) - (u-u_0)\sin u_0 \cos u]q_0 - \\ \qquad [\sin(u-u_0) - (u-u_0)\cos u_0 \cos u]k_0 - \\ \qquad [(1+\beta)/2](u-u_0)[2\sin u - (u-u_0)\cos u], \\ k(u) = [\sin(u-u_0) - (u-u_0)\sin u_0 \sin u]q_0 + \\ \qquad [\cos(u-u_0) + (u-u_0)\cos u_0 \sin u]k_0 + \\ \qquad [(1+\beta)/2](u-u_0)[2\cos u + (u-u_0)\sin u], \end{cases} \tag{3.4b}$$

$$\begin{cases} q(u) = \{\tilde{S}_\alpha(u)[\sin(u-u_0) - \alpha\cos u_0 \sin u] + \tilde{C}_\alpha(u)\cos(u-u_0)\}q_0 + \\ \qquad \{\tilde{S}_\alpha(u)[\cos(u-u_0) - \alpha\sin u_0 \sin u] - \tilde{C}_\alpha(u)\sin(u-u_0)\}k_0 - \\ \qquad (\alpha+\beta)\tilde{S}_\alpha(u)\sin u + [(\alpha+\beta)/(1-\alpha)][1 - \tilde{C}_\alpha(u)]\cos u, \\ k(u) = \{-\tilde{S}_\alpha(u)[\cos(u-u_0) - \alpha\cos u_0 \cos u] + \tilde{C}_\alpha(u)\sin(u-u_0)\}q_0 + \\ \qquad \{\tilde{S}_\alpha(u)[\sin(u-u_0) + \alpha\sin u_0 \cos u] + \tilde{C}_\alpha(u)\cos(u-u_0)\}k_0 + \\ \qquad (\alpha+\beta)\tilde{S}_\alpha(u)\cos u + [(\alpha+\beta)/(1-\alpha)][1 - \tilde{C}_\alpha(u)]\sin u, \end{cases} \tag{3.4c}$$

Plugging (3.4) into (3.3) we obtain the formulae of the radius vector for (a) $\alpha < 1$, (b) $\alpha = 1$, and (c) $\alpha > 1$:

$$r = p_0\left[\frac{1+\beta}{1-\alpha} - \Big(\frac{\alpha+\beta}{1-\alpha} - e_0\cos v_0\Big)C_\alpha(u) - e_0\sin v_0 S_\alpha(u)\right]^{-1}, \tag{3.5a}$$

$$r = p_0\left[\frac{1+\beta}{2}(u-u_0)^2 - e_0\sin v_0(u-u_0) + 1 + e_0\cos v_0\right]^{-1}, \tag{3.5b}$$

$$r = p_0\left[-\frac{1+\beta}{\alpha-1} + \Big(\frac{\alpha+\beta}{\alpha-1} + e_0\cos v_0\Big)\tilde{C}_\alpha(u) - e_0\sin v_0\tilde{S}_\alpha(u)\right]^{-1}, \tag{3.5c}$$

where $e_0 = (q_0^2 + k_0^2)^{1/2}$, $v_0 = u_0 - \arctan(k_0/q_0)$ stay for initial conditions. These formulae are equivalent with (2.6).

IV. RELATIONSHIP BETWEEN TIME AND POLAR ANGLE

In the previous section we have described the evolution of the radius vector as a function of the argument of latitude. To complete the integration of the equations (3.1), we will determine the function $t = t(u)$, which allows us to express the solution as a function of the time variable. For this, consider first the following notations:

$$\bar{A} = \frac{(1-\alpha)e_0\cos v_0 - (\alpha+\beta)}{1+\beta},\ \bar{B} = \frac{(1-\alpha)^{\frac{1}{2}}e_0\sin v_0}{1+\beta},\ \tilde{B} = \frac{(\alpha-1)^{\frac{1}{2}}e_0\sin v_0}{1+\beta},$$

$$K = 2(1-\alpha)^{\frac{3}{2}}(1+\beta)^{-2},\ \tilde{K} = 2(\alpha-1)^{\frac{3}{2}}(1+\beta)^{-2},$$

$$e^* = (\bar{A}^2+\bar{B}^2)^{\frac{1}{2}},\ w = (1-e^{*2})^{\frac{1}{2}},\ \tilde{w} = (e^{*2}-1)^{\frac{1}{2}},$$

$$f(u) = \cot[(1/2)\sqrt{1-\alpha}(u-u_0)],\ \tilde{f}(u) = \coth[(1/2)\sqrt{\alpha-1}(u-u_0)],$$

$$X(u) = (\bar{A}+1)f(u) - \bar{B},\ Y(u) = (\bar{A}+e^{*2})f(u) - \bar{B},\ Z(u) = w^2 + X^2(u),$$

$$\tilde{X}(u) = (\bar{A}+1)\tilde{f}(u) + \tilde{B},\ \tilde{Y}(u) = (\bar{A}+e^{*2})\tilde{f}(u) + \tilde{B},\ \tilde{Z}(u) = w^2 - \tilde{X}^2(u),$$

$$x = 1 + e_0\cos v_0,\ y = -e_0\sin v_0,\ D = 2(1+\beta)x - y^2,$$

$$\hat{X}(u) = \frac{2[(1+\beta)x - y^2](u-u_0) - (1+\beta)y(u-u_0)^2}{x[2x + 2y(u-u_0) + (1+\beta)(u-u_0)^2]},$$

$$\hat{Y}(u) = \frac{u-u_0}{2x + y(u-u_0)},\ \hat{Z}(u) = \frac{(1+\beta)(u-u_0)}{2y[y + (1+\beta)(u-u_0)]}.$$

Direct computations give us the following relations in each of the cases (a) $\alpha < 1$, (b) $\alpha = 1$, (c) $\alpha > 1$, respectively:

$$\begin{cases} t = t_0 + (Kp_0^{3/2}/w^3\sqrt{\mu})[\arctan(w/X(u)) - wY(u)/Z(u)], & \text{for } e^* < 1, \\ t = t_0 + (Kp_0^{3/2}/3\sqrt{\mu})[(2+3X(u)f(u))/X^3(u)], & \text{for } e^* = 1, \\ t = t_0 + (Kp_0^{3/2}/\tilde{w}^3\sqrt{\mu})[\tilde{w}Y(u)/Z(u) - \operatorname{arg\,tanh}(\tilde{w}/X(u))], & \text{for } e^* > 1, \end{cases} \tag{4.1a}$$

$$\begin{cases} t = t_0 - \frac{p_0^{3/2}}{D\sqrt{\mu}}[\hat{X}(u) + (2(1+\beta)/\sqrt{-D})\operatorname{arg\,tanh}(\sqrt{-D}\hat{Y}(u))], & \text{for } D < 0, \\ t = t_0 + 4p_0^{2/3}\hat{Z}(u)/\sqrt{\mu}, & \text{for } D = 0, \\ t = t_0 + \frac{p_0^{3/2}}{D\sqrt{\mu}}[\hat{X}(u) + (2(1+\beta)/\sqrt{D})\arctan(\sqrt{D}\hat{Y}(u))], & \text{for } D > 0, \end{cases} \tag{4.2b}$$

$$\begin{cases} t = t_0 + (\tilde{K}p_0^{3/2}/w^3\sqrt{\mu})[\operatorname{arg\,tanh}(w/\tilde{X}(u)) + w\tilde{Y}(u)/\tilde{Z}(u)], & \text{for } e^* < 1, \\ t = t_0 + (\tilde{K}p_0^{3/2}/3\sqrt{\mu})[(3\tilde{X}(u)\tilde{f}(u) - 2)/\tilde{X}^3(u)], & \text{for } e^* = 1, \\ t = t_0 + (\tilde{K}p_0^{3/2}/\tilde{w}^3\sqrt{\mu})[\tilde{w}\tilde{Y}(u)/\tilde{Z}(u) + \arctan(\tilde{w}/\tilde{X}(u))], & \text{for } e^* > 1. \end{cases} \tag{4.1c}$$

Relations $p = p_0, \Omega = \Omega_0, i = i_0$, (3.4), and (4.1) give now, in closed form, the solution of the equations of motion (3.2) of the Manev problem.

V. BLOW UP AND REDUCTION

To begin our qualitative endeavors, let us write the Manev problem as a Hamiltonian system, as at the beginning of Section II, with a Hamiltonian of the type

$$H(\mathbf{p},\mathbf{q}) = \frac{1}{2}(|\mathbf{p_1}|^2 + |\mathbf{p_2}|^2) - \frac{1}{|\mathbf{q}_1 - \mathbf{q}_2|} - \frac{k}{|\mathbf{q}_1 - \mathbf{q}_2|^2}, \tag{5.1}$$

where the units (including those of the masses) have been chosen such that the constants A and B take the values 1 and k, respectively.

Considering polar coordinates $r > 0$, $\theta \in S^1$, where S^1 is the segment $[0, 2\pi]$ with the end points identified, the Hamiltonian takes the form

$$H(p_r, p_\theta, r) = (1/2)(p_r^2 + p_\theta^2/r^2) - 1/r - k/r^2, \tag{5.2}$$

where p_r, p_θ are the new polar variables.

To blow up the collision singularity that occurs at $r = 0$ we formally multiply the energy integral by r^2 (a detailed justification of this step was given in the local study near the collision performed in a previous paper that uses McGehee transformations (see ref. 11)). The energy relation takes now the form

$$(1/2)r^2 p_r^2 + p_\theta^2 - r - k = hr^2. \tag{5.3}$$

Introducing further the transformations $v = rp_r$ and $u = p_\theta$ and scaling the time variable by using $dt = r^2 d\tau$, the equations given by the Hamiltonian (5.2), take the form

$$\begin{cases} r' = rv \\ v' = r(1 + 2hr) \\ \theta' = u \\ u' = 0, \end{cases} \tag{5.4}$$

having the energy relation (5.3) transformed into

$$v^2 + u^2 - 2r - 2hr^2 = 2k. \tag{5.5}$$

The prime denotes here differentiation with respect to the new, fictitious, time variable τ.

Define the *collision manifold* as the set of solutions given by relation (5.5) when $r = 0$. Notice that, geometrically, the collision manifold is a cylinder in the three-dimensional space of the coordinates (u, θ, v), and since $\theta \in [0, 2\pi]$, it follows that this cylinder can be identified with a torus. In fact, the two-dimensional torus representing the collision manifold is imbedded in the full four-dimensional phase space of the coordinates (r, u, θ, v). The equations (5.4) show that the flow on the collision manifold is formed almost exclusively by periodic orbits, except the upper and lower circles of the torus given by $r = 0$, $u = 0$, $v = \pm\sqrt{2k}$, which consist of equilibrium points (see Figure 2a).

Figure 2.
(a) The collision manifold imbedded in the four-dimensional phase space.
(b) The collision manifold in the reduced phase space.

Since θ does not appear explicitly in the equations (5.4) or in the energy relation (5.5), we can further reduce the four-dimensional phase space to dimension three by factorizing the flow to S^1. Exploiting this symmetry (characteristic to this problem), we will obtain clear pictures of the global flow in phase space. In what follows we will describe the global reduced flow as well as the flow in phase space, by regarding the energy as a parameter.

Factorizing the collision manifold to S^1, the torus becomes a circle (see Figure 2b). The points M and N on this circle correspond to the circles of equilibria on the torus, while all the other points correspond to the periodic orbits on the torus.

VI. ORBITS OF ELLIPTIC TYPE

In this section we consider negative-energy case, $h < 0$. Let us first write the energy relation (5.5) in a convenient way, as

$$v^2 + u^2 - 2h(r + 1/2h)^2 = 2k - 1/2h, \tag{6.1}$$

which shows that, in the reduced phase space, every energy level is a two-dimensional sphere (in the three-dimensional Euclidean space (r, v, u) with $r \geq 0$ (see Figure 3)). In other words, every negative-energy level is homeomorphic with a two-dimensional disk. The boundary of this disk is $r = 0$, $v^2 + u^2 = 2k$, i.e. the circle that defines the collision manifold.

Figure 3.
The flow on each negative-energy level.

The analysis of the equations (5.4) allows us to describe the flow on the negative-energy levels. There are two equilibria outside the collision manifold, located at $r = -1/2h$, $v = 0$, $u = \pm\sqrt{2k - 1/2h}$. Since u is a first integral all solutions are represented by curves lying in parallel planes, $u =$ constant. Therefore, depending on the constant value of u, the orbits are heteroclinic if $|u| < \sqrt{2k}$, homoclinic for $u = \pm\sqrt{2k}$, and periodic for $\sqrt{2k} < |u| < \sqrt{2k - 1/2h}$. Note that in the unreduced phase space all these "orbits" are in fact manifolds. Each manifold consists of the product between an "orbit" and S^1.

The physical interpretation in each of these cases is as follows. The heteroclinic orbit connecting M and N corresponds to rectilinear solutions starting from a collision and ending in a collision. They are homothetic orbits. All the other heteroclinic orbits connecting equilibria of the collision circle are, in full phase space, heteroclinic orbits between the periodic orbits on the collision torus. Physically they also correspond to solutions ejecting from collision and then tending to collision, but the collision is not rectilinear anymore: the particle colliding with the center spirals around the center. There

are, in fact, infinitely many rotations before collision, as we will prove in Section VII. The homoclinic orbits in Figure 3 correspond in full phase space to orbits ejecting from the *big* circle of the torus and returning to it and to orbits ejecting from the *small* cicle of the torus and returning to it. (The *big* and *small* circles are the ones in the "equatorial" plane $v = 0$.) Their physical interpretation is similar to that of the heteroclinic ones that spiral at ejection-collision. As we have already proved in ref. 11, this also shows that there exists a set of positive measure of initial data that leads to collisions.

The case of periodic orbits, for $\sqrt{2k} < |u| < \sqrt{2k - 1/2h}$, is the most interesting one from the mathematical point of view. In full phase space each of these orbits corresponds to a linear flow on a torus: $S^1 \times S^1$. Each torus is therefore filled with either periodic or with quasiperiodic orbits (this is a well-known fact in the qualitative theory of dynamical systems[18]). It is the goal of Section VII to find the frequency ratio and prove that most of the tori are filled with quasiperiodic orbits and that only a negligible set of them consists of tori foliated by periodic orbits. Physically, the quasiperiodic solutions correspond to precessional ellipses that fill an annulus densely, whereas the periodic ones are either elliptic orbits or precessional orbits that close after a finite number of rotations.

The last case to dicuss is that of the two equilibria outside the collision manifold at $r = -1/2h$, $v = 0$, $u = \pm\sqrt{2k - 1/2h}$. In full phase space they correspond to periodic orbits, and are elliptic orbits in physical space. This completes the description of the negative-energy case.

VII. PERIODIC AND QUASIPERIODIC ORBITS

In this section we want to determine the nature of the tori of orbits in the previous section. For this we will compute the frequency ratio, which will tell us whether the corresponding orbits are periodic or quasiperiodic. Periodic orbits correspond to rational ratios, whereas quasiperiodic ones correspond to irrational ratios.

Let $\rho = \sqrt{-2h}(r + \frac{1}{2h})$, and observe that $\rho = \frac{1}{\sqrt{-2h}} = \alpha$ represents collision. From the equations of motion (5.4) we get

$$\rho' = (\rho + 1/\sqrt{-2h})v$$
$$v' = -\rho(\rho + 1/\sqrt{-2h}).$$

Now observing that

$$v^2 + \rho^2 = 2k - \frac{1}{2h} - u^2 = I^2,$$

we introduce polar coordinates (I, ϕ) in the (ρ, v) plane. Notice that

$$\phi' = \frac{v\rho' - \rho v'}{\rho^2 + v^2} = \rho + \alpha = I\sin\phi + \alpha.$$

Taking now $z = \tan\frac{\phi}{2}$, the equivalent equation

$$d\tau = \frac{d\phi}{I\sin\phi + \alpha}$$

takes the form

$$d\tau = \frac{2dz}{\alpha z^2 + 2Iz + \alpha} = \frac{2dz}{\alpha[(z + I/\alpha)^2 + 1 - I^2/\alpha^2]}.$$

Note that $I < \alpha$ corresponds to noncollision orbits. Integrating the last equation, we obtain

$$\tau = \frac{2}{a\alpha} \arctan \frac{z + I/\alpha}{a} + constant,$$

where $a = \sqrt{1 - I^2/\alpha^2}$.

The period T is given by

$$T = \tau|_0^T = \int_0^{2\pi} F(\phi) d\phi,$$

where the right hand side is a (convergent) improper integral at $\phi = \pi$. Then

$$T = \frac{4}{a\alpha} \lim_{\phi \to \pi} \left[\arctan \frac{I/\alpha + \tan \phi/2}{a} - \arctan \frac{I}{a\alpha} \right] = \frac{2}{a\alpha} \left[\pi - 2 \arctan \frac{I}{a\alpha} \right],$$

and after replacing the values of α, a, and I we get

$$T = \frac{2\sqrt{-2h}}{\sqrt{2h(2k - u^2)}} \left[\pi - 2 \arctan \frac{\sqrt{1 + 2h(u^2 - 2k)}}{\sqrt{2h(2k - u^2)}} \right].$$

Notice now that if $\rho \to \alpha$, then $a \to \infty$ and $T \to \infty$. Also, if $I \to 0$, then $a \to 1$ and $T \to \frac{2\pi}{\alpha}$.

Finally, the frequency ratio of the torus is

$$\frac{T}{u} = \frac{2}{u\sqrt{u^2 - 2k}} \left[\pi - 2 \arctan \frac{\sqrt{1 + 2h(u^2 - 2k)}}{\sqrt{2h(2k - u^2)}} \right].$$

It becomes clear now that, for fixed k, most of the values taken by the frequency ratio, as a continuous function of u, are irrational. This proves that, except for a set of measure zero of tori foliated by periodic orbits, most of the tori are generated by quasiperiodic orbits.

VIII. ORBITS OF PARABOLIC AND HYPERBOLIC TYPE

Let us finally consider the zero-energy, $h = 0$, and the positive-energy, $h > 0$, cases. In the zero-energy case, the energy relation takes the form

$$v^2 + u^2 = 2r + 2k,$$

which implies that the zero-energy level is a paraboloid with the cap removed (see Figure 4). (The cap is removed because $r \geq 0$.) From the topological point of view this is

the complement of a disk bordered by the collision circle, i.e. an annulus. Again, the first integral $u = \ constant$, foliates the zero-energy level into curves lying in parallel planes. The curves are either parabolas, for $|u| \geq \sqrt{2k - 1/2h}$, or arcs of parabolas, for $|u| < \sqrt{2k - 1/2h}$. There are no equilibria outside the collision circle.

Figure 4.
The flow in the zero-energy case

The physical interpretation of the orbits corresponding to the arc of parabola tending to N or ejecting from M is that of rectilinear orbits that come from (or tend to) infinity with asymptotic velocity zero. The other orbits corresponding to arcs of parabolas that tend to (or eject from) the collision circle, is that of precessional parabolas that spiral at collision (ejection) and have asymptotic velocity zero at infinity. The orbits corresponding to parabolas do not encounter collisions and are precessional parabolas with asymptotic velocity zero at infinity.

In the positive-energy case, the energy relation takes the form

$$v^2 + u^2 - 2h(r + 1/2h)^2 = 2k - 1/2h.$$

Depending on the relation between h and k, three possibilities arise: (1) $h < 1/4k$, (2) $h = 1/4k$, and (3) $h > 1/4k$.

In case (1), the energy relation describes a hyperboloid of one sheet intersected with $r \geq 0$ (see Figure 5a). The first integral, $u = constant$, foliates the surface in branches of hyperbolas or arcs of branches of hyperbolas and two pairs of lines (which correspond to the points F and G). The physical interpretation is similar to that of the zero-energy case, just that parabolas are now substituted by branches of hyperbolas and the asymptotic velocity at infinity is not zero but positive.

Figure 5
The flows in the three cases of the positive-energy levels.

In case (2), the energy relation is a cone intersected with $r \geq 0$ (see Figure 5b), and the first integral $u = constant$ foliates the surface in branches of hyperbolas or arcs of branches of hyperbolas and two half-lines (those corresponding to M and N). The physical interpretation of the corresponding orbits is similar to the one of the previous case, (1).

In case (3), the energy relation is a hyperboloid of two sheets intersected with $r \geq 0$, i.e. one sheet with the cap removed (see Figure 5c). The first integral $u = constant$ foliates the surface in branches of hyperbolas and arcs of branches of hyperbolas. The physical interpretation of the corresponding orbits is the same as in case (1) above.

This gives the complete picture of the Manev problem.

ACKNOWLEDGEMENTS

Florin Diacu and Angelo Mingarelli were supported in part by the grants OGP0122045 and OGP0114651 of the National Science and Engineering Research Council of Canada,

while Joaquín Delgado, Ernesto Lacomba, and Ernesto Perez received partial support from Conacyt Grant 1772-E9210.

REFERENCES

[1]Maneff, G., La gravitation et le principe de l'égalité de l'action et de la réaction, Comptes Rendus **178** (1924), 2159-2161; Die Gravitation und das Prinzip von Wirkung und Gegenwirkung, Zeitschrift für Physik **31** (1925), 786-802; Le principe de la moindre action et la gravitation, Comptes Rendus **190** (1930), 963-965; La gravitation et l'énergie au zéro, Comptes Rendus **190** (1930), 1374-1377.
[2]Lacomba, E.A., Llibre J. and Nunes A., Invariant tori and cylinders for a class of perturbed Hamiltonian systems, in The Geometry of Hamiltonian Systems, Proceedings of a Workshop held June 5-16, 1989, T. Ratiu, ed., Springer Verlag, New York, 1991.
[3]Mioc, V., Elliptic-type motion in Fock's gravitational field, Astron. Nachr. **315** (1994), 175-180.
[4]Saslaw, W.C., Motion around a source whose luminosity changes, Astrophys. Journ. **226** (1978), 240-252.
[5]Mioc, V. and Radu, E., Orbits in an anisotropic radiation field, Astron. Nachr. **313** (1992), 353-357.
[6]Şelaru, D., Cucu-Dumitrescu, C. and Mioc, V., On a two-body problem with periodically changing equivalent gravitational parameter, Astron. Nachr. **313** (1992), 257-263.
[7]Moulton, F.R., An Introduction to Celestial Mechanics, (second revised edition) Dover, New York, 1970, pp. 119-122.
[8]Ureche, V., Free-fall collapse of a homogeneous sphere in Maneff's gravitational field, Rom. Astron. Journ. **5** (1995) (to appear).
[9]Diacu, F.N., Near-collision dynamics for particle systems with quasihomogeneous potentials, Journ. Differential Equations (1996) (to appear).
[10]Diacu, F.N., The planar isosceles problem for Maneff's gravitational law, Journ. Math. Phys. **34** (12) (1993), 5671-5690.
[11]Diacu, F.N., Mingarelli, A., Mioc, V. and Stoica, C., The Manev two-body problem: quantitative and qualitative theory, in Dynamical Systems and Appliations, World Scinetific Series in Applicable Analysis, vol. 4, World Scientific, Singapore, 1995 (to appear).
[12]Craig, S., Diacu, F.N., Lacomba, E. and Perez, E., The anisotropic Manev problem (in preparation).
[13]McGehee, R., Triple collision in the collinear three-body problem, Inventiones math. **27** (1974), 191-227.
[14]Duboshin, G.N.: Celestial Mechanics. Basic Problems and Methods, Gos. Izd. Fiz.-Mat. Lit, Moscow, 1963 (in Russian), pp. 351-380.
[15]Schneider, M.: Himmelsmechanik, Bd.2, BI Wissenschaftverlag, Mannheim, Wien, 1993. pp. 152-157.

[16]Samoilovich, G.V.: A system of parameters for the description of space-vehicle orbits, ISZ 16 (1963) 136-139 (in Russian).
[17]Appell, P.: Cours de Mécanique, 3e éd., Gauthier-Villars, Paris, 1912, p. 294.
[18]Robinson, C.: Dynamical Systems: Stability, Dynamical Systems, and Chaos, CRC Press, Boca Raton, Florida, 1995.

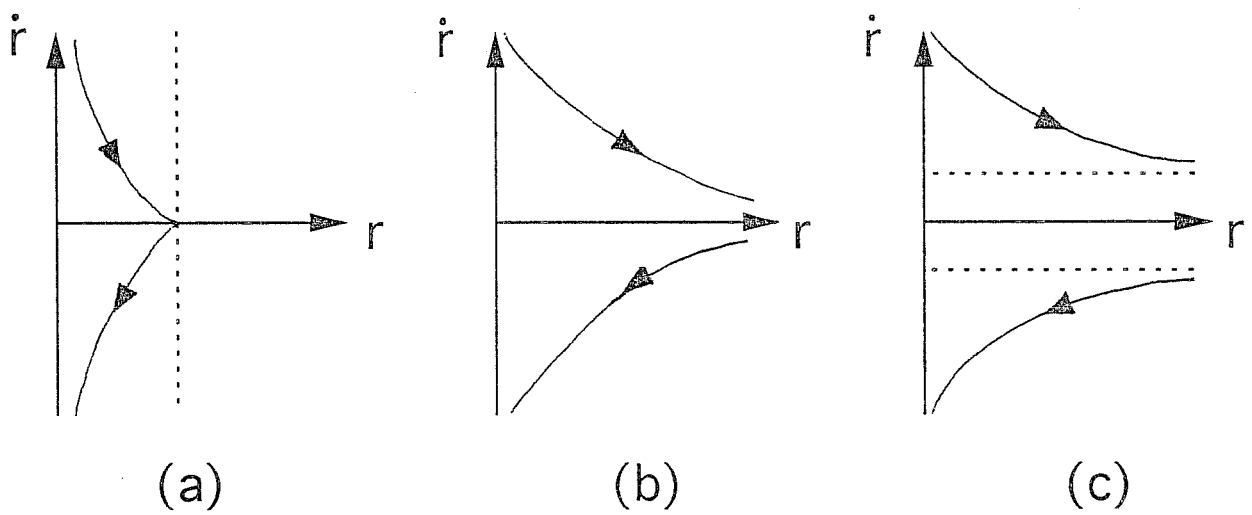

Figure 1

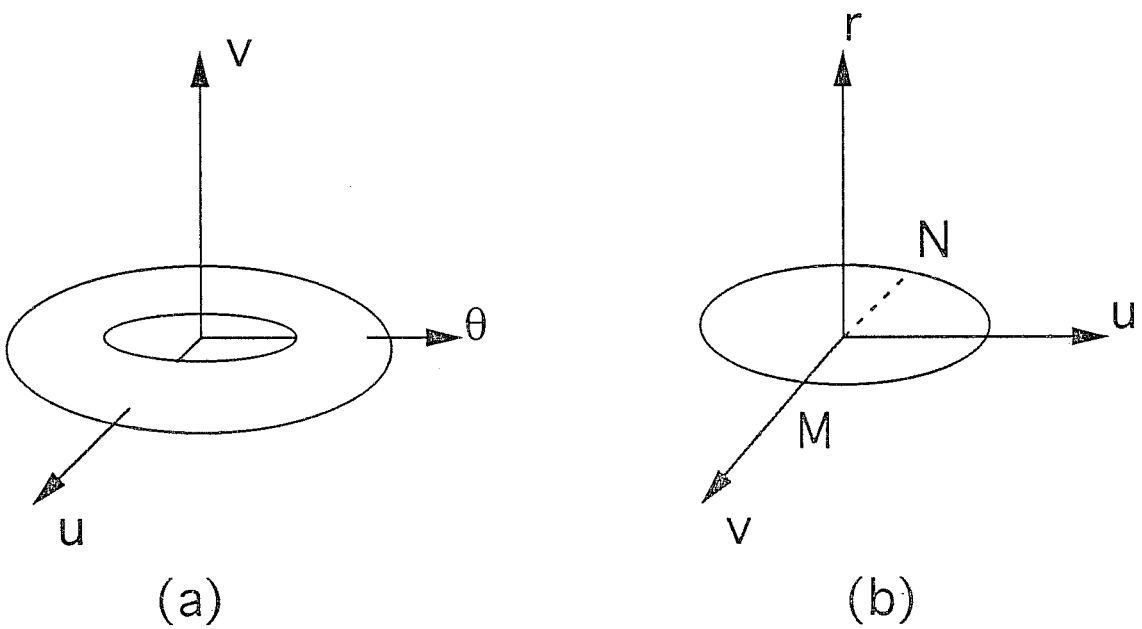

Figure 2

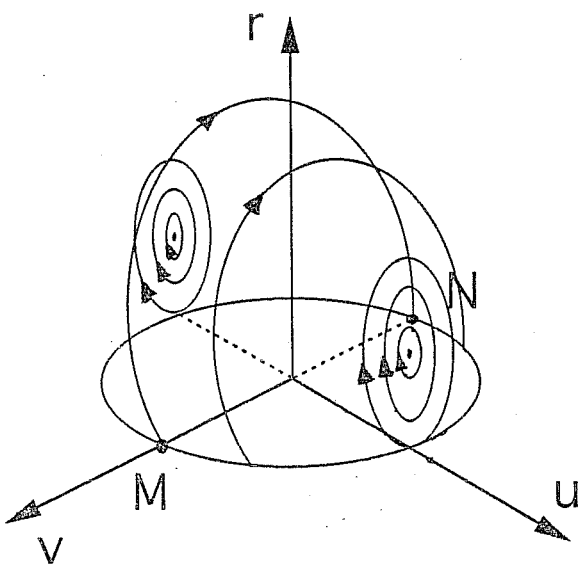

Figure 3

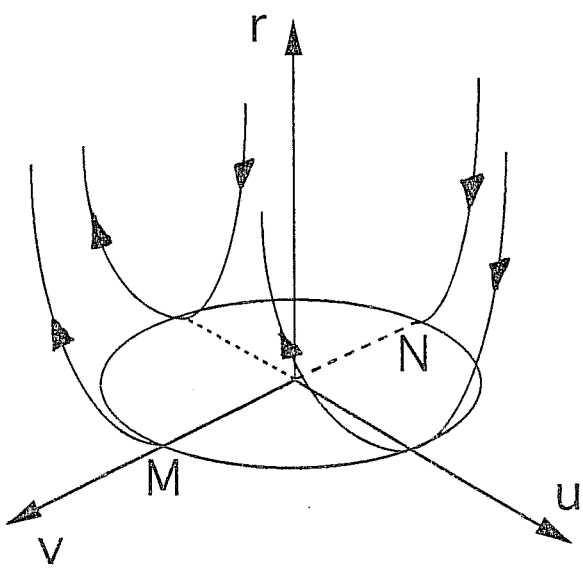

Figure 4

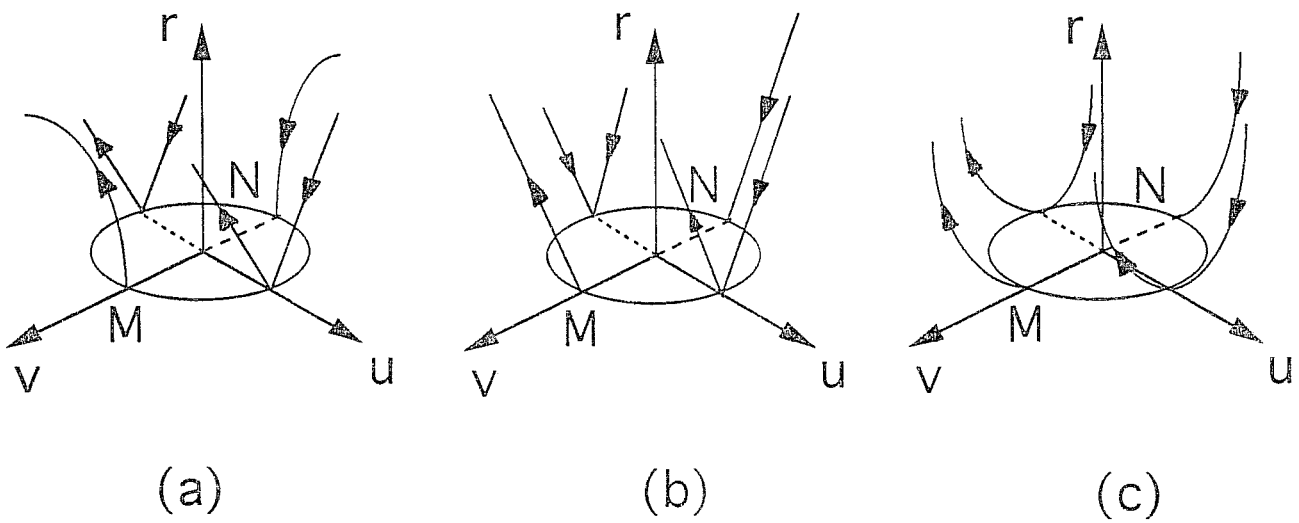

Figure 5